



PERSPECTIVE

Resonant nano-electromechanical systems from 2D materials

To cite this article: Kai-Ming Hu *et al* 2020 *EPL* **131** 58001

View the [article online](#) for updates and enhancements.

You may also like

- [Erratum: Simultaneous observation of small- and large-energy-transfer electron-electron scattering in three-dimensional indium oxide thick films](#)
Yang Yang, Xin-Dian Liu and Zhi-Qing Li
- [Erratum: On variational arguments for vibrational modes near jamming](#)
Le Yan, Eric DeGiuli and Matthieu Wyart
- [Erratum: State-of-the-art techniques for calculating spectral functions in models for correlated materials](#)
K. Hallberg, D. J. García, Pablo S. Cornaglia et al.

Perspective

Resonant nano-electromechanical systems from 2D materials

KAI-MING HU, PENG BO, XIU-YUAN LI, YI-HANG XIN, XIN-RU BAI, LEI LI and WEN-MING ZHANG^(a)

*State Key Laboratory of Mechanical System and Vibration, School of Mechanical Engineering,
Shanghai Jiao Tong University - Shanghai 200240, China*

received 26 June 2020; accepted in final form 26 August 2020

published online 18 September 2020

PACS 85.85.+j – Micro- and nano-electromechanical systems (MEMS/NEMS) and devices

PACS 03.65.Sq – Semiclassical theories and applications

PACS 05.45.-a – Nonlinear dynamics and chaos

Abstract – Intriguing mechanical properties of two-dimensional (2D) atomically thin materials make them well suit for a new class of resonant NEMS. Resonant 2D NEMS show high fundamental frequencies, outstanding tenability and broad dynamic range due to the ultrahigh strength, ultralow mass density and ultrahigh strain stretchability. Recent work toward exploring fabrication and transduction techniques, device performances and the nonlinear dynamic characteristics of 2D NEMS are summed up. Nonlinear dynamic behaviors including nonlinear mode coupling, nonlinear damping and nonlinear pull-in instability are reported in 2D NEMS.

perspective

Copyright © 2020 EPLA

Introduction. – Because of remarkable mechanical, electronic and optical properties, 2D nanomaterials, atomically perfect crystals, have been considered as promising materials for a variety of fundamental researches including nonlinear damping [1–5], mode coupling [6–9], geometric nonlinearity [10–12], and nanodevice applications, such as mass sensing [13–15], force sensing [16], radio frequency (RF) signal processing [17–20]. The nanodevices from 2D materials can be divided into quasistatic and resonant NEMS. 2D materials are typically contacted with the substrates in the former devices; for the latter, 2D material sheets are usually suspended over the substrates. In the review, we pay close attention to the resonant NEMS from 2D materials.

Compared with one-dimensional NEMS [21–24], 2D NEMS have several advantages and provide unprecedented opportunities for realizing atomically thin transducers. Firstly, ultrathin membrane structures of 2D materials have high elastic modulus, ultimately low mass density, and those outstanding mechanical properties make them attractive for fabricating very-high-frequency (VHF) resonant 2D NEMS. Secondly, 2D planar functional structures with atomic layer thickness can bring larger active area, which is essential for mass, pressure and gas sensing. Thirdly, 2D nanodevices have greater linear dynamic range (DR) and superb intrinsic flexibility up to 25%

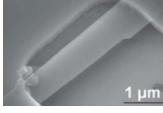
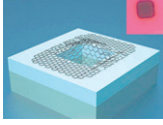
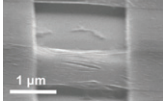
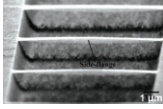
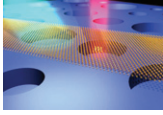
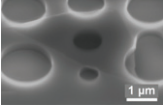
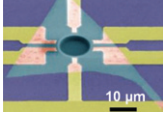
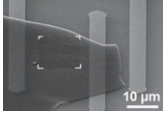
enabling high-frequency tunable 2D resonators [25]. Moreover, thin membrane structures allow 2D NEMS compatible with surface patterning processes and are suitable for large-scale production [26].

However, nanoscale characteristic size in the thickness direction (1 nm–100 nm) imposes many new challenges for resonant 2D NEMS, which are different from the mainstream MEMS [27–29]. The fabrication of 2D NEMS is a quite different branch, most of the “top-down” micro-fabrication technologies are not applicable to 2D NEMS. Integrating mature MEMS technologies into bottom-up NEMS devices is an interesting yet challenging topic [27]. Moreover, the actuation and detection of 2D NEMS become more difficult due to low signal-to-noise ratio, and the dynamical tuning range is usually extremely limited [25]. In addition, the nonlinear dynamic behaviors, such as nonlinear internal resonance, nonlinear damping and mode coupling, are more easily triggered in 2D NEMS.

This paper reviews the state-of-the-art technologies and perspectives of 2D NEMS. We first summarize the main fabrication processes of resonant 2D NEMS. The actuation and detection schemes including capacitive, piezoresistive and optical transductions of resonant 2D nanodevices are briefly described. Furthermore, we also reviewed the dynamic modeling of 2D NEMS. Finally, the intrinsic properties and interesting nonlinear dynamic behaviors of resonant NEMS are discussed.

^(a)E-mail: wenmingz@sjtu.edu.cn

Table 1: The main materials, fabrications, transductions and performances of 2D NEMS.

Materials	Fabrication	Actuation	Detection	f (MHz)	Q	$f \times Q$	DR (dB)	Device image
Graphene [30]	exfoliation	electrical /optical	optical	70	78 (in vacuum)	5×10^9	60	
Graphene [31]	exfoliation	optical	optical	66	25 (in gas)	1.6×10^9	–	
Graphene [32]	CVD	electrical /optical	electrical /optical	75	9000 (at 9 K)	6.7×10^{11}	–	
Graphene [33]	epitaxial growth	optical	optical	100	400	1.0×10^{10}	–	
MoS ₂ [25]	exfoliation	electrical /optical	electrical /optical	120	1000	1.2×10^{11}	70–110	
MoS ₂ [34]	CVD	optical	optical	120	250	3×10^{10}	–	
BN [35]	exfoliation	optical	optical	70	619	4.3×10^{10}	70–110	
Black phosphorus [36]	exfoliation	optical	optical	75.7	120	9.1×10^9	–	

Fabrication technology. – The main fabrication techniques of 2D NEMS are reviewed in this section. Since the first 2D material, graphene, is discovered by mechanical exfoliation technique [28], many other 2D atomic layer crystalline membranes are fabricated by different producing processes, as listed in table 1. The 2D materials used in NEMS can be divided into zero-gap graphene [27], 2D semiconductor materials (MoS₂, other TMDCs and black phosphorus) [29,37,38], 2D dielectric materials (h-BN) [35,39] and 2D van der Waals heterostructures [40,41], which can be fabricated by mechanical exfoliation, chemical vapor deposition (CVD) growth and epitaxial growth methods. In this section, we

focus on the suspended technologies of 2D membranes, which can make nanodevices free to resonate.

Suspended techniques. The key procedure to fabricate resonant NEMS is to suspend 2D membranes over the target substrates. For 2D materials produced by mechanical exfoliation, CVD and epitaxial growth, three approaches can be employed to suspend 2D membranes. The first technique is exfoliating and optically locating 2D materials onto the top of pre-patterned substrates to acquire well-suspended sheets. Bunch *et al.* [30] firstly used mechanically exfoliated graphene sheets to fabricate doubly clamped rectangular 2D NEMS resonators over

pre-patterned trenches with length from 0.5 to 10 μm . This method can protect 2D materials from contamination since it does not require the complex transfer processes or wet etching processes.

The second technique is that 2D materials are firstly exfoliated onto substrates, then electrodes are patterned and supported structures are released to make 2D membranes suspend with wet etching processes [42]. Shivaraman *et al.* [33] released doubly clamped graphene membranes by removing the underneath SiC by photoelectrochemical wet etching process. In this method, the wet etching process can make 2D thin membranes difficult to well suspend over the holes or trenches.

Moreover, to produce suspended 2D NEMS, 2D thin flakes are transferred from initial substrates to target substrates. The transfer techniques can be classified into the wet and dry transfer methods. In the wet transfer method, the carrier materials, such as polymethyl methacrylate (PMMA) [43–45] or polydimethylsiloxane (PDMS) [46], are spin-coated onto 2D flakes/metal substrates and the metal substrates are chemically etched in the solution. The carrier material/2D material structures are first transferred into the liquid and then wet transferred onto the target substrates with predefined trenches. van der Zande *et al.* [32,47] employed this transfer technique to fabricate large-scale integration of NEMS-based 2D materials. However, the 2D membranes are apt to stick into the bottom of trenches due to liquid tension [43]. To eliminate the influence of liquid tension, the dry transfer techniques are developed to the well-suspended structures of 2D NEMS [38,48–50]. Suk *et al.* [48] proposed a reproducible dry transfer technique to allow large-area CVD graphene to be transferred over microchambers and the carrier material was removed by annealing in a furnace with Ar and H_2 at 350 $^\circ\text{C}$ for ~ 2 h.

Buried gate techniques. Gate electrode configurations can greatly affect the electrical and dynamical performances of 2D NEMS. The back-gate structure, using a substrate as a gate, has been widely utilized in 2D NEMS because it is easy to fabricate [14,30]. The substrate can apply an electric field to suspended 2D membranes, but the contact resistance is varied when the electrostatically actuated NEMS works. Jiang *et al.* [51] demonstrated magnetic resonators by transferring 2D CrI_3 on prefabricated circular microtrenches with patterned Au electrodes and Si back gate.

Another way is to adopt additional metal gate electrodes [6,7]. Barton *et al.* [52] fabricated gate electrodes, which covered the whole trenches in graphene resonators by e-beam evaporation of 5 nm Ti/25 nm Pt. Moreover, Manzeli *et al.* [13] implemented a local gate to reduce the parasitic effects in high-frequency monolayer MoS_2 NEMS. Lee *et al.* [17,53] introduced a layer of silicon oxide or PMMA on the top of electrodes to bury the local gate.

Built-in strain. The residual built-in strains of suspended flakes in 2D NEMS are apt to generate during

the fabrication process, such as chemical modification, strain mismatch due to different thermal expansion coefficients [15], and the wet transfer techniques [43,44]. Moreover, because 2D flakes have atomic thinness and the bending rigidity is extremely small, the resonant frequency of 2D NEMS can be strongly impacted by the built-in strain [27]. Therefore, it is essential to evaluate the built-in strain and the corresponding membrane bending. Hu *et al.* [54] developed a theoretical model considering different thermal expansion coefficients between 2D flakes and substrates to evaluate the built-in strain and transverse deflection during the fabrications.

Actuation and detection schemes. – As the size of NEMS shrinks, the actuation and detection of mechanical vibrations become a central challenge. The optical, electrostatic, and piezoresistive transduction techniques employed in 2D nanodevices are briefly described.

Capacitive transduction scheme. In the capacitive transduction of resonant NEMS in fig. 1(a), the charge-dependent conductance of 2D materials can be utilized to transduce the high-frequency vibrations of 2D membranes to the time-varying electrical signals [14]. The mainstream electrical readout techniques include direct transduction, two-source frequency mixing and one-source or frequency modulation mixing [1,32]. To overcome the drawback of large parasitic capacitance, the two-source frequency mixing technique is proposed to downmix the radio-frequency signal to a much lower frequency [32,55]. Although the mixing technique has been proven to be useful, the measurement bandwidth is quite limited, which can cause this method to be very time consuming and is not suitable for RF applications. Xu *et al.* [56] reported RF electrical readout of graphene mechanical resonators, which employed a local gate electrode in the etched trench to greatly minimize parasitic capacitance. To increase measurement speed, Song *et al.* [57] proposed another method to successfully improve the sensitivity of the RF cavity readout scheme and detect resonant frequency in the gigahertz range, which employed a π -matching network coupled with local gates.

Optical transduction scheme. As shown in fig. 1(b), two laser beams are used for actuation and detection of 2D NEMS, respectively [58]. The suspended 2D sheets are driven photothermally using the laser, which can cause periodic contraction/expansion of the 2D materials and lead to vibrational motions. Another laser beam is employed for detection, the substrate acts as the fixed mirror, while the suspended membranes act as the moving mirror (fig. 1(b)). The intensity modulation of the reflected signal can be used to detect the mechanical vibration of 2D NEMS.

The advantage of this scheme is that it can transduce the vibrational motion of any suspended 2D structures without introducing complex electrodes [36,52,59]. Electrical mixing techniques can be utilized to detect graphene NEMS, however, those techniques are challenging to apply

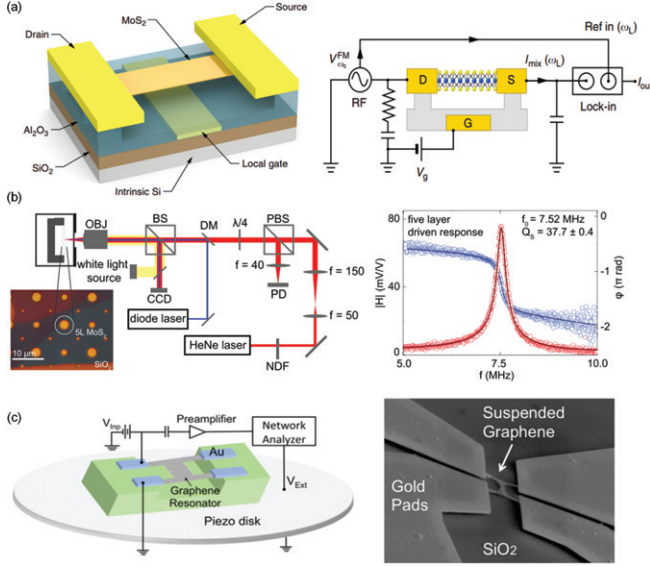


Fig. 1: The main transduction schemes of resonant 2D NEMS: (a) all-electrical actuation and detection technique [13]; (b) optical transduction [58]; (c) piezoresistive transduction [64].

to semiconducting TMD NEMS because the high electrical resistance of devices can cause a lot of Joule heating. To reduce heating, Morell *et al.* [50] adopted ultralow laser power down to 70 nW to detect mechanical vibrations of WSe₂ resonators by optical interferometry.

Piezoresistive transduction scheme. The piezoresistivity of 2D materials can be used for an effective sensing method in 2D NEMS [60–63]. As shown in fig. 1(c), by utilizing the intrinsic piezoresistivity of graphene as a self-sensing component, Kumar and Bhaskaran [64] proposed an ultrasensitive piezoresistive transduction of graphene NEMS. To maximize the piezoresistivity, a four-sided clamped H-shaped suspended graphene beam resonator is fabricated to measure across the regions of maximum stress near the supports of the mechanical beam (fig. 1(c)). The results demonstrated that the piezoresistive transduction scheme to sense the vibration of monolayer graphene resonators is robust, repeatable, and sensitive enough to even detect the second mode of resonance [64].

Scanning force microscopy scheme. Additionally, a direct method is developed to image the mechanical vibrations of 2D NEMS. García-Sánchez *et al.* [65] reported a novel form of scanning force microscopy (SFM) to detect the motions of suspended graphene membranes driven by RF voltages, which allowed identification and imaging of the spatial shape of the eigenmodes. The advantage of this detection method can directly image the mode shape of 2D NEMS. However, because the SFM is usually served in the air, the quality factors (Q) of the nanodevices are quite low.

Dynamic modelling. – For 2D material membrane or nanoribbon structures in resonant NEMS, different

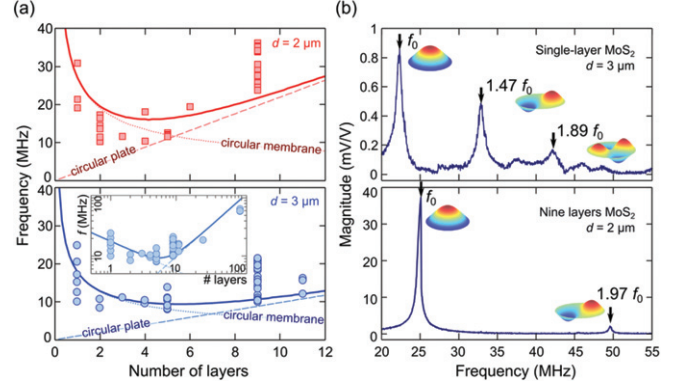


Fig. 2: Resonant frequency with respect to the number of layers for MoS₂ mechanical resonators [38].

mechanical models can be used to characterize of dynamic properties of 2D nanodevices. According to the geometric configurations and layer number, 2D NEMS can be divided into membrane-like, plate-like, membrane/plate mixed, and beam-like devices [29,66].

Tension-dominated membrane regime. The resonant structures of 2D NEMS are typically very thin and the bending rigidity is too small to be ignored, especially for the monolayer or bilayer 2D materials. For a membrane-like NEMS, the fundamental frequency f_m can be expressed by [38]

$$f_m = \frac{2.405}{\pi d} \sqrt{\frac{T}{\rho t}}, \quad (1)$$

where ρ , t and d denote the mass density, thickness and diameter of 2D structures, respectively; T is the initial tension. For resonant MoS₂ NEMS in fig. 2, eq. (1) is suitable for sheets thinner than 3–4 layers.

Elasticity-dominated plate regime. When the layer number of 2D materials increases, the bending rigidity cannot be ignored and the elastic membrane theory is not applicable. For a plate-like circular NEMS, the first mode frequency f_p can be written as [38]

$$f_p = \frac{10.21}{\pi} \sqrt{\frac{E}{3\rho(1-\nu^2)}} \frac{t}{d^2}, \quad (2)$$

where E and ν are Young's modulus and Poisson's ratio of the 2D materials, respectively. For resonant MoS₂ NEMS in fig. 2, eq. (2) is suitable for flakes thicker than 10–12 layers.

Membrane and plate mixed regime. When the thickness of 2D structures increases, the 2D NEMS have a transition from membrane behavior to plate behavior. For resonant MoS₂ NEMS in fig. 2, the flakes with 4 to 10 layer thickness are in this crossover regime. For 2D NEMS in the membrane and plate mixed regime, the resonance frequency f_{mix} can be obtained as [38]

$$f_{\text{mix}} = \sqrt{f_m^2 + f_p^2}. \quad (3)$$

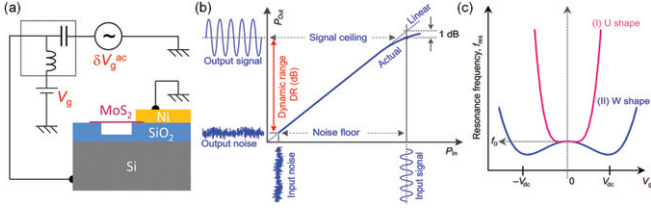


Fig. 3: VHF MoS₂ nanoelectromechanical resonators with wide-range electrical tenability: (a) schematic of electrical tuning; (b) illustration of DR; (c) two types of frequency tuning [25].

Beam regime. For the NEMS with 2D strip-like nanoribbons, the resonant frequency can be given by [65]

$$f_b = \frac{1.028}{l^2} \sqrt{\frac{Et^2}{\rho}} + T \frac{0.154}{\sqrt{\rho E w^2 t^4}}, \quad (4)$$

where l and w are the length and width of NEMS, respectively.

Intrinsic properties. –

Frequency tuning. The resonant frequency of 2D NEMS can be tuned over a wide range by external excitations due to the ultrathin thickness and superflexibility of 2D materials. The strong dependence of frequency on the membrane tension can provide an effective way to wide-range resonant frequency tuning. Chen *et al.* [17] have demonstrated that the frequency can be adjusted up to 400% by the gate voltage. As shown in fig. 3(a), the relationship of resonant frequency to the gate voltage can be expressed as [25]

$$f_v = \frac{1}{2\pi} \sqrt{\left[4.9EtT + \frac{\pi\epsilon_0}{8(1-\nu^2)} \frac{d^2}{EtT^2} V_g^4 - \frac{\pi\epsilon_0 d^2}{3g^3} V_g^2 \right] / M_{\text{eff}}}, \quad (5)$$

where ϵ_0 and g denote the vacuum permittivity and gap depth, V_g and M_{eff} are the gate voltage and effective mass, respectively.

As indicated in eq. (5), the second term represents the spring constant hardening due to the gate voltage-controlled tension; the third term represents a spring constant softening due to the nonlinear electrostatic force. For small initial tension, the second term dominates, the frequency increases with V_g , monotonically, and the “U”-shape frequency tuning curve was observed in fig. 3(c) [25]. For large initial tension, the third term will dominate and the frequency decreases with V_g , monotonically [56]. For initial tension in the crossover regime, the frequency firstly decreases and then increases with V_g , and the “W”-shape frequency tuning curve was observed in fig. 3(c) [25].

Quality factor. Another performance of 2D NEMS is the quality factor, which can be defined as

$$Q = 2\pi E_t / \Delta E_d, \quad (6)$$

where E_t and ΔE_d denote the total energy stored and the energy dissipated per cycle in the resonant NEMS, respectively.

High Q indicates that the damping of NEMS is very small and the resonance peak is very sharp, which is critical for the applications of resonant devices. The size and supporting boundaries of 2D membranes can greatly impact the Q due to the supporting loss. Barton *et al.* [47] demonstrated that Q in tensile graphene resonators is highly related to the diameter of the membranes. Moreover, the Q of 2D drummed NEMS with fully clamped structures is typically higher than that in NEMS with doubly clamped beams [67]. At room temperature, the Q of the doubly clamped graphene resonators by mechanical exfoliation or CVD are indicated as 80–300 [17,30], nevertheless, the Q of fully clamped graphene resonators is about 2400 [47].

Additionally, the operating temperature can strongly affect the Q of 2D NEMS, which is caused by temperature-dependent dissipation. The relationship of dissipation to temperature has two different stages: $Q^{-1} \propto T_e^2$ when the temperature is above 100 K, $Q^{-1} \propto T_e^{0.3-0.4}$ when the temperature is below 100 K [17,32].

Frequency- Q product. Although the resonant frequencies of 2D NEMS increase with the decreasing size of devices, Q are seriously affected. For better evaluation of device performance, frequency- Q product ($f \times Q$) is defined. Using ultraclean suspended and current-annealed graphene p - n junctions, Jung *et al.* [68] reported a GHz nanomechanical resonator with $f \times Q = 1.8 \times 10^{12} \text{ s}^{-1}$ at temperature of 8 K. Compared to the graphene NEMS, the $f \times Q$ of 2D semiconductor NEMS resonators is larger because the 2D semiconductor materials exhibit lower intrinsic energy dissipation than graphene [69]. Morell *et al.* [50] fabricated a WSe₂ resonator with high quality factor and $f \times Q = 2.7 \times 10^{12} \text{ s}^{-1}$.

Dynamic range. Large DR of resonant NEMS is a critical and desirable performance parameter. As shown in fig. 3(b), DR can be defined as the ratio between the highest signal level prior to any nonlinear bifurcation (“signal ceiling”) and the lowest detectable level (“noise floor”) [66]. The linear DR of 2D NEMS defined by the ratio between the 1 dB compression point and the noise floor can be expressed as [25]

$$DR \equiv 20 \log \left(\frac{0.745a_c}{\sqrt{2S_{x,\text{th}}\Delta f}} \right), \quad (7)$$

where a_c and Δf are the critical amplitude triggering bistability and measurement bandwidth, respectively, $S_{x,\text{th}}$ is the displacement-domain spectral density. Wang *et al.* [66] demonstrated that the intrinsic DR depends on the device parameters including size, layer number and initial built-in tension.

Nonlinear dynamic behaviors. – The nonlinearity, such as stiffness softening and hardening, nonlinear mode

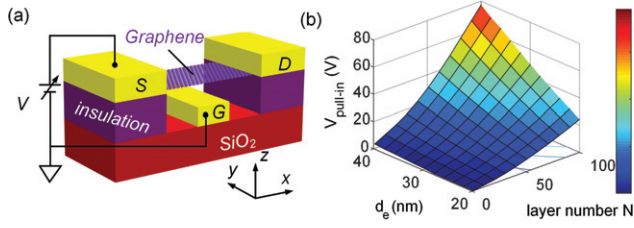


Fig. 4: (a) Schematics of suspended graphene sensors, where S, D and G denote source, drain and gate electrodes, respectively. (b) The 3D dispersion curve of pull-in voltage $V_{\text{pull-in}}$ as a function of electrode gap distances d_e and layer number N [54].

coupling and nonlinear damping of 2D NEMS become more easily triggered when the size of the devices reduces to the nanoscale. Therefore, it is important to understand the nonlinear dynamic behaviors of the devices for their performance design and optimization [10–12].

Nonlinear mode coupling. The strong nonlinear coupling between different mechanical modes observed in NEMS can be used for VHF sensing, low-noise oscillators and tuning nonlinear dynamic performances [70,71]. By applying large strain, Samanta *et al.* [8] observed the strong nonlinear coupling between different vibrational modes in MoS₂ resonators, which makes the devices an attractive tool to study the nonlinear dynamics and quantum mechanics. Moreover, Liu *et al.* [9] indicated that the extent of mode softening can control intermode energy exchange in the strong-coupling regime. The tension-mediated nonlinear coupling between various modes of the resonator can be excited in a controllable manner and strong coupling between mechanical modes is adjusted using detuned pumps [6].

Moreover, the strong mode coupling effects among electronic, optical, magnetic properties and mechanical motion have been reported in 2D NEMS, which can result in the fields of cavity quantum electromechanics [72,73] and cavity optomechanics [74–77]. Zhang *et al.* [74,75] studied coherent phonon dynamics between spatially separated graphene mechanical resonators, in which the coupling between well-separated mechanical modes can be manipulated via a phonon cavity. Therefore, 2D NEMS can be an effective tool for probing quantum-limited phenomena and quantum information processing technologies.

Nonlinear damping. When the dimensions of the devices range from the metre-scale to the nanoscale, the simple linear damping model is not suitable for characterizing the energy dissipation behaviors of 2D NEMS [76]. Eichler *et al.* [1] demonstrated that the damping of graphene-based NEMS is strongly dependent on the vibrational amplitude. By adjustment of the driving power to avoid nonlinear damping, Q as high as 100000 is obtained. Croy *et al.* [2] attributed the microscopic mechanism of nonlinear damping to the coupling between flexural modes

and in-plane phonons in graphene resonators. Moreover, a negative nonlinear damping mechanism is observed in a multilayer graphene mechanical resonator at large amplitudes [3]. The damping of the MoS₂ drum resonator is found to be strain-dependent and microscopic wrinkles of 2D membranes could also play a role in the strong dissipation of devices [5]. In addition, Lee *et al.* [4] investigated the air damping effects on the resonance frequencies and Q in MoS₂ resonators.

Nonlinear pull-in instability. As shown in fig. 4(a), an external electric field is commonly adopted to adjust the dynamic performance of 2D NEMS. However, the high external gate voltage can result in the pull-in instability of devices due to the small bending rigidity of 2D sheets [15,49]. Using a Fredholm integral equation, Rokni and Lu [77] investigated the effects of surface tension and elasticity on the pull-in instability of graphene ribbons. Moreover, Hu *et al.* [54] developed an electromechanical model to characterize nonlinear pull-in behaviors of suspended graphene sensors, which indicates that the axial prestress can be a controllable way to improve the pull-in stability (fig. 4(b)).

Conclusions and potential applications. – We briefly reviewed the state-of-the-art of resonant 2D NEMS including the fabrication, actuation and detection technologies, dynamical models and intrinsic properties of devices. The interesting nonlinear dynamic behaviours of 2D NEMS are also highlighted. Furthermore, resonant 2D NEMS show tremendous potential applications, such as RF signal processing [17–19,78], mass sensing [13–15], pressure sensing [16,61,62,79] and applications in the quantum regime [80].

The authors gratefully acknowledge the support by National Science Foundation for Distinguished Young Scholars (Grant No. 11625208), the Program of Shanghai Academic/Technology Research Leader (19XD1421600), National Natural Science Foundation of China (Grant No. 11802173), the China Postdoctoral Science Foundation (2018M632103) and Postdoctoral Innovative Talent support program (BX20180190).

REFERENCES

- [1] EICHLER A. *et al.*, *Nat. Nanotechnol.*, **6** (2011) 339.
- [2] CROY A. *et al.*, *Phys. Rev. B*, **86** (2012) 235435.
- [3] SINGH V. *et al.*, *Phys. Rev. B*, **93** (2016) 245407.
- [4] LEE J. *et al.*, *Appl. Phys. Lett.*, **105** (2014) 023104.
- [5] KRAMER E. *et al.*, *Appl. Phys. Lett.*, **107** (2015) 091903.
- [6] MATHEW J. P. *et al.*, *Nat. Nanotechnol.*, **11** (2016) 747.
- [7] GUTTINGER J. *et al.*, *Nat. Nanotechnol.*, **12** (2017) 631.
- [8] SAMANTA C. *et al.*, *Appl. Phys. Lett.*, **107** (2015) 173110.
- [9] LIU C.-H. *et al.*, *Nano Lett.*, **15** (2015) 6727.
- [10] SAMANTA C. *et al.*, *Nanoscale*, **11** (2019) 8394.
- [11] SAMANTA C. *et al.*, *Appl. Phys. Lett.*, **113** (2018) 113101.

- [12] CHOWDHURY A. *et al.*, *Nat. Commun.*, **11** (2020) 1.
- [13] MANZELI S. *et al.*, *Nat. Commun.*, **10** (2019) 1.
- [14] CHEN C. *et al.*, *Nat. Nanotechnol.*, **4** (2009) 861.
- [15] SUN J. *et al.*, *Sci. Adv.*, **2** (2016) e1501518.
- [16] DOLLEMAN R. J. *et al.*, *Nano Lett.*, **16** (2016) 568.
- [17] CHEN C. *et al.*, *Nat. Nanotechnol.*, **8** (2013) 923.
- [18] ZHOU Q. *et al.*, *Proc. Natl. Acad. Sci. U.S.A.*, **112** (2015) 8942.
- [19] VERBIEST G. J. *et al.*, *Nano Lett.*, **18** (2018) 5132.
- [20] ZHOU Q. and ZETTL A., *Appl. Phys. Lett.*, **102** (2013) 223109.
- [21] HU K. M. *et al.*, *Phys. Lett. A*, **378** (2014) 650.
- [22] HU K. M. *et al.*, *J. Vib. Acoust.*, **138** (2015) 011020.
- [23] ZHANG W.-M. *et al.*, *J. Phys. D: Appl. Phys.*, **49** (2016) 165304.
- [24] URGELL C. *et al.*, *Nat. Phys.*, **16** (2020) 32.
- [25] LEE J. *et al.*, *Sci. Adv.*, **4** (2018) eaao6653.
- [26] WANG M. Z., in *2016 IEEE-NANO* (IEEE) 2016, pp. 875–878.
- [27] CHEN C. and HONE J., *Proc. IEEE*, **101** (2013) 1766.
- [28] NOVOSELOV K. S. *et al.*, *Science*, **306** (2004) 666.
- [29] LEE J. *et al.*, *ACS Nano*, **7** (2013) 6086.
- [30] BUNCH J. S. *et al.*, *Science*, **315** (2007) 490.
- [31] BUNCH J. S. *et al.*, *Nano Lett.*, **8** (2008) 2458.
- [32] VAN DER ZANDE A. M. *et al.*, *Nano Lett.*, **10** (2010) 4869.
- [33] SHIVARAMAN S. *et al.*, *Nano Lett.*, **9** (2009) 3100.
- [34] JIA H. *et al.*, *Nanoscale*, **8** (2016) 10677.
- [35] ZHENG X. Q. *et al.*, *Microsyst. Nanoeng.*, **3** (2017) 1.
- [36] WANG Z. *et al.*, *Nanoscale*, **7** (2015) 877.
- [37] LEE J. *et al.*, *Nanoscale*, **8** (2016) 7854.
- [38] CASTELLANOS-GOMEZ A. *et al.*, *Adv. Mater.*, **25** (2013) 6719.
- [39] CARTAMIL-BUENO S. J. *et al.*, *npj 2D Mater. Appl.*, **1** (2017) 1.
- [40] YE F. *et al.*, *Nanoscale*, **9** (2017) 18208.
- [41] WILL M. *et al.*, *Nano Lett.*, **17** (2017) 5950.
- [42] STOLYAROVA E. *et al.*, *Nano Lett.*, **9** (2009) 332.
- [43] HU K.-M. *et al.*, *Small*, **15** (2019) 1804337.
- [44] HU K.-M. *et al.*, *Carbon*, **152** (2019) 233.
- [45] HU K.-M. *et al.*, *Adv. Funct. Mater.*, **30** (2020) 2003273.
- [46] KIM K. S. *et al.*, *Nature*, **457** (2009) 706.
- [47] BARTON R. A. *et al.*, *Nano Lett.*, **11** (2011) 1232.
- [48] SUK J. W. *et al.*, *ACS Nano*, **5** (2011) 6916.
- [49] LIU X. *et al.*, *Adv. Mater.*, **26** (2014) 1571.
- [50] MORELL N. *et al.*, *Nano Lett.*, **16** (2016) 5102.
- [51] JIANG S. *et al.*, arXiv preprint, arXiv:2001.03153 (2020).
- [52] BARTON R. A. *et al.*, *Nano Lett.*, **12** (2012) 4681.
- [53] GUAN F. *et al.*, *Appl. Phys. Lett.*, **107** (2015) 266601.
- [54] HU K.-M. *et al.*, *EPL*, **125** (2019) 20011.
- [55] SINGH V. *et al.*, *Nanotechnology*, **21** (2010) 165204.
- [56] XU Y. *et al.*, *Appl. Phys. Lett.*, **97** (2010) 243111.
- [57] SONG X. *et al.*, *Nano Lett.*, **12** (2012) 198.
- [58] VAN LEEUWEN R. *et al.*, *Appl. Phys. Lett.*, **105** (2014) 041911.
- [59] RESERBAT-PLANTEY A. *et al.*, *Nat. Nanotechnol.*, **7** (2012) 151.
- [60] SMITH A. D. *et al.*, *Nano Lett.*, **13** (2013) 3237.
- [61] ZHU S.-E. *et al.*, *Appl. Phys. Lett.*, **102** (2013) 161904.
- [62] SMITH A. D. *et al.*, *ACS Nano*, **10** (2016) 9879.
- [63] MANZELI S. *et al.*, *Nano Lett.*, **15** (2015) 5330.
- [64] KUMAR M. and BHASKARAN H., *Nano Lett.*, **15** (2015) 2562.
- [65] GARCÍA-SÁNCHEZ D. *et al.*, *Nano Lett.*, **8** (2008) 1399.
- [66] WANG Z. and FENG P. X. L., *Appl. Phys. Lett.*, **104** (2014) 103109.
- [67] KIM S. Y. and PARK H. S., *Nano Lett.*, **9** (2009) 969.
- [68] JUNG M. *et al.*, *Nanoscale*, **11** (2019) 4355.
- [69] JIANG J.-W. *et al.*, *Nanoscale*, **6** (2014) 3618.
- [70] ERIKSSON A. M. *et al.*, *Nanotechnology*, **24** (2013) 395702.
- [71] HU K.-M. *et al.*, *J. Vib. Acoust.*, **137** (2015) 021008.
- [72] SINGH V. *et al.*, *Appl. Phys. Lett.*, **100** (2012) 233103.
- [73] RESERBAT-PLANTEY A. *et al.*, *Nat. Commun.*, **7** (2016) 1.
- [74] LUO G. *et al.*, *Nat. Commun.*, **9** (2018) 383.
- [75] ZHANG Z.-Z. *et al.*, *Proc. Natl. Acad. Sci. U.S.A.*, **117** (2020) 5582.
- [76] MATIS B. R. *et al.*, *Sci. Rep.*, **7** (2017) 1.
- [77] ROKNI H. and LU W., *J. Appl. Phys.*, **113** (2013) 153512.
- [78] MIAO T. *et al.*, *Nano Lett.*, **14** (2014) 2982.
- [79] WEBER P. *et al.*, *Nat. Commun.*, **7** (2016) 1.
- [80] CHEN C. *et al.*, *Nat. Phys.*, **12** (2016) 240.